LiFS: Low Human-Effort, Device-Free Localization with Fine-Grained Subcarrier Information

Ju Wang[†], Hongbo Jiang[‡], Jie Xiong[♯], Kyle Jamieson[§],
Xiaojiang Chen[†], Dingyi Fang[†], Binbin Xie[†]
[†]Northwest University; [‡]Huazhong University of Science and Technology; [♯]Singapore Management University;
[§]Dept. of Computer Science, Princeton University and University College London
[†]{wangju,xjchen,dyf}@nwu.edu.cn, [‡]hongbojiang2004@gmail.com,
[♯]jxiong@smu.edu.sg, [§]kylej@cs.princeton.edu, [†]bbx@stumail.nwu.edu.cn

ABSTRACT

Device-free localization of people and objects indoors not equipped with radios is playing a critical role in many emerging applications. This paper presents an accurate model-based device-free localization system *LiFS*, implemented on cheap commercial off-the-shelf (COTS) Wi-Fi devices. Unlike previous COTS device-based work, LiFS is able to localize a target accurately without offline training. The basic idea is simple: channel state information (CSI) is sensitive to a target's location and by modelling the CSI measurements of multiple wireless links as a set of power fading based equations, the target location can be determined. However, due to rich multipath propagation indoors, the received signal strength (RSS) or even the fine-grained CSI can not be easily modelled. We observe that even in a rich multipath environment, not all subcarriers are affected equally by multipath reflections. Our pre-processing scheme tries to identify the subcarriers not affected by multipath. Thus, CSIs on the "clean" subcarriers can be utilized for accurate localization.

We design, implement and evaluate LiFS with extensive experiments in three different environments. Without knowing the majority transceivers' locations, LiFS achieves a median accuracy of 0.5 m and 1.1 m in line-of-sight (LoS) and non-line-of-sight (NLoS) scenarios respectively, outperforming the state-of-the-art systems. Besides single target localization, LiFS is able to differentiate two sparsely-located targets and localize each of them at a high accuracy.

Categories and Subject Descriptors

C.2.1 [**Computer-Communication Networks**]: Network Architecture and Design–*Wireless communication*

Keywords

Device-Free Localization; Channel State Information; Low Human-Effort; Multipath; Power Fading Model

MobiCom'16, October 03-07, 2016, New York City, NY, USA

DOI: http://dx.doi.org/10.1145/2973750.2973776

1. INTRODUCTION

We have witnessed an ever-increasing roll-out of location-based applications, such as indoor localization [45, 43], shop navigation [27, 1], augmented reality [29, 11], etc, for which location information is the key. Most current localization systems [14, 25, 44, 42], however, require the person to carry a device (such as a mobile phone), making them a poor fit for some applications. For instance, in intrusion detection [38, 49], expecting an uncooperative target to carry a device is not realistic. In elderly care, the aged are reluctant to wear a wearable device or bring a mobile [20]. As such, device-free localization without any device attached to the target has attracted a lot of research efforts recently [2, 46].

Among all the technologies employed for indoor localization, Wi-Fi is still considered one of the most promising schemes due to its ubiquity. Wi-Fi is widely used to connect a wide range of devices, such as mobiles, laptops and loudspeakers in modern offices and homes. This provides us a large number of Wi-Fi links around us. Ideally, we want to passively localize a target with only these existing Wi-Fi links without any additional infrastructure.

Traditional device-free localization systems (or approaches) are mainly based on the coarse-grained RSS signatures [49, 32, 5, 22], resulting in a limited localization accuracy [38, 48, 34]. To improve accuracy, fine-grained CSI fingerprint[1]-based systems have been proposed recently [40, 47]. In order to achieve a high localization accuracy, these systems (i) need a comprehensive site survey to build the detailed fingerprint database, and (ii) require updating the database from time to time because in a real indoor environment, the radio-frequency (RF) signals vary due to environmental changes. The site survey and frequent database update incur a prohibitively-high human cost, rendering them impractical for real-life deployment. These existing systems also assume that all the transceivers' locations are known and remain unchanged. As a result, they will encounter large localization errors if the locations of transceivers (such as mobile phones) change, since the change of a Wi-Fi link would lead to the fingerprints in the database not matching the measured CSI readings.

On the other hand, raw CSI measurements from COTS devices can not be directly applied to model a target's location because of strong multipath propagations and hardware

[1]A fingerprint is a unique feature of the signal related to the location, such as RSS or CSI.

noise. Thus, the previous approaches [40, 47] have difficulties employing a unified model to accurately quantify the relationship between the CSI measurement and the target's location. As a result, they require a significant amount of human efforts to manually build and update a fingerprint database frequently. If we can quantify the relationship between the target location and the CSI measurement with a model, many applications would benefit, bypassing the labor-intensive training process. In intruder tracking scenario, we can localize the intruders in an unfamiliar scenario that is not likely to have a pre-obtained fingerprint database.

In this paper, we present LiFS, an accurate model-based device-free localization system with low human effort. LiFS does not rely on an exhaustive fingerprint database and only requires baseline measurements between transceivers. That is to say, the amount of human efforts for LiFS is very small compared with measuring or updating the RSS/CSI signatures at all possible locations in existing fingerprint-based location systems. Without knowing the locations of all transceivers, LiFS is able to achieve a high localization accuracy (sub-meter level), while most existing device-free localization systems exhibit a coarse accuracy.

To remove the noise on raw CSI measurements, we observe that not all subcarriers are affected equally by multipaths even in a rich multipath environment. Consequently, we introduce a novel CSI pre-processing method to filter out those subcarriers greatly affected by multipath and hardware noise. After this processing, we can quantify the relationship between the pre-processed CSI values and a target's locations with the help of a power fading model (PFM).[2] With such a relationship, LiFS can calculate a target's location without requiring any labor-intensive offline training.

LiFS still faces the challenge that the locations of some transceivers (such as mobile phones, laptops, etc.) are unknown, since a target's location estimate is related to the transceivers' locations in the PFM. To address this challenge, LiFS establishes a set of equations with the help of the PFM to restrict the locations of both the target and the transceivers with unknown locations. *The key observation is that the number of unknown transceivers grows linearly while the number of PFM equations grows in a quadratic fashion.* This implies that with enough Wi-Fi links, the equation constraints will be sufficient to localize both the unknown transceivers and the target.

To further illustrate the key concept of LiFS, Fig. 1 shows a toy example with one target and five transceivers (i.e., three APs, one mobile phone and one laptop). We assume the mobile's location is unknown, so the total number of unknowns is four since both the mobile and the target have two unknown parameters, namely their $[x, y]$ coordinates in 2D space. The total number of Wi-Fi links is six (3×2) so we can establish six PFM equations. Thus there are enough constraints to localize the target and the mobile phone in this example.

Although the idea sounds straightforward, it is non-trivial to solve the PFM equations efficiently due to the complex non-linear Fresnel integration in PFM [21]. To handle this, we seek an optimization solution that minimizes the mean absolute error between the CSI measurements and the PFM-calculated CSI values. To this end, we use a hybrid approach

[2]The power fading model [21] describes the relationship between the power fading, i.e., the CSI amplitude, and the distances between the target and the two transceivers.

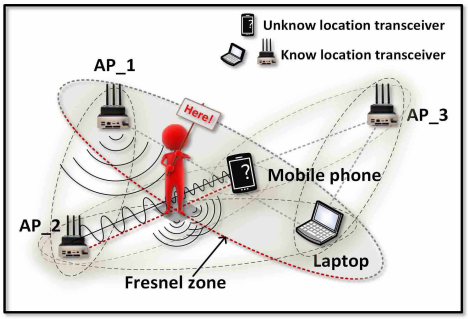

Figure 1: A toy example of localization with LiFS.

that starts with the genetic algorithm [18] by picking an initial set of solutions[3] efficiently without a local minima, and then refine the solution employing the gradient descent [4] scheme to reach the final location estimate.

We build a prototype of LiFS employing 11 laptops, each equipped with an Intel 5300 NIC [8]. Four of them serve as access points (APs) with the "hostapd" tool [17], and the rest serve as clients. Note that we do not include the links between clients as we only assume access to CSI data from APs. The target to be passively localized is a human without any device attached. Our experimental results demonstrate that, even in a challenging situation when the locations of 6 out of all the 7 clients are unknown, LiFS achieves a median accuracy of 0.5 m and 1.1 m in LoS and NLoS scenarios respectively for a single target, outperforming the state-of-the-art systems. For two targets, LiFS can still localize each individual target accurately when the targets are 1.8 m apart. Note that passively localizing more than one target is a well-known challenging problem [48].

Contributions: The main contributions of this paper are as follows:

1. We propose a novel CSI pre-processing scheme to select those "clean" subcarriers, which conform to the proposed model, thus ensure a high localization accuracy even in rich multipath environment.
2. By modelling the device-free localization problem as a set of over-determined equations, LiFS does not need to know the locations of all the transceivers and is able to determine their locations together with the target.
3. LiFS is implemented on commercial off-the-shelf hardware and extensive experiments demonstrate the effectiveness of the system.

Paper outline: We review the related work in Section 2. The system overview is described in Section 3. We introduce the background in Section 4. We describe the pre-processing scheme and the localization method in Section 5 and Section 6, respectively. The implementation of LiFS is described in Section 7. LiFS is evaluated and discussed in Section 8 and Section 9, followed by a conclusion in Section 10.

2. RELATED WORK

There are growing interests in exploring RF for device-free localization. Compared with camera or infrared based solutions [16, 13], RF-based device-free localization approaches can work at day and night, and also can penetrate non-metallic walls [48]. Recently, a lot of fine-grained RF-based

[3]A solution consists of a vector of all the unknowns, i.e., the locations of a target and the transceivers with unknown locations.

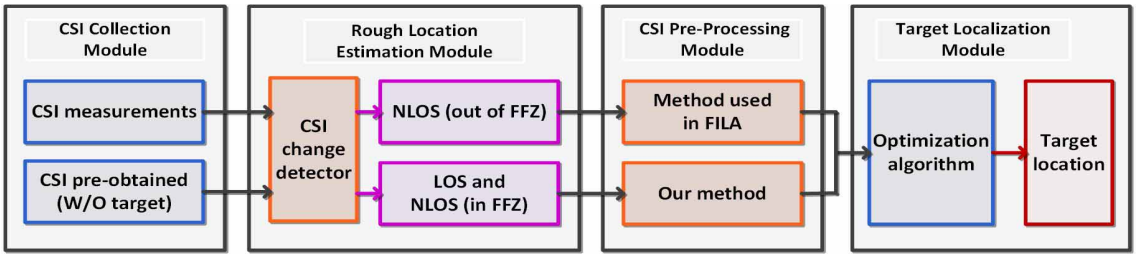

Figure 2: System overview of LiFS.

localization systems have been proposed, such as Wi-Vi [3], WiDeo [12], Witrack2.0 [2], mtrack [37], Tadar [46], etc. These methods, though being able to achieve a high accuracy, require dedicated hardware such as USRPs to send out specialized frequency modulated carrier wave signal [2] or special purpose device to generate 60 GHz signal [37] or a customized RFID reader with a tag array [46].

On the other hand, several RSS-based device-free localization systems have been proposed [38, 49, 32, 48, 34], achieving the goal of low hardware cost for localization as RSS readings are widely available in commercial off-the-shelf Wi-Fi devices. However, RSS is inherently a coarse measurement [9] and strong multipath makes the problem even worse [39]. As such, RSS-based device-free localization techniques have difficulties providing high localization accuracy in most home/office environments [2, 40].

Compared with RSS, CSI measurements provide more fine-grained information on each subcarrier with both amplitude and phase information for device-free detection and localization [50, 40, 47]. To localize a target, many systems utilize the CSI measurements as unique signatures of a target's locations [40, 47]. However, these systems suffer from labor-intensive offline training since they need a comprehensive site survey to build and update the detailed fingerprint database. LiFS does not need any training effort, and only requires the baseline measurements between transceivers which is a very small workload. CSI has also been employed in gesture and activity recognition systems [36, 35, 28, 6, 19].

Additionally, most existing device-free localization proposals including RSS-based [38, 49] and CSI-based [40, 47] rely on the assumption that the locations of all transceivers are known and unchanged. In reality, this assumption could be easily violated since users may move their devices. With enough transceiver pairs, LiFS can determine the locations of both the unknown transceivers and the target, eliminating the necessity of knowing all the transceivers' locations.

3. SYSTEM OVERVIEW

LiFS is a model-based device-free localization system that can localize a target accurately with low human effort. LiFS acquires CSI measurements from the existing Wi-Fi infrastructure, and assumes the locations of APs are known. LiFS does not need to know the locations of all the clients (e.g., mobiles) involved for locating a target, and can determine their locations together with the target. LiFS is composed of the following four modules as shown in Fig. 2:

- **CSI Collection Module:** Before the target moves into the monitoring area, LiFS collects a set of CSI measurements (i.e., baseline data) from all the links. LiFS then acquires another set of CSI measurements from all the links when a target moves into the area.
- **Rough Location Estimation Module:** LiFS detects whether the target is present in the First Fresnel Zone (FFZ) of a specific link by comparing the currently measured CSI value with the pre-obtained CSI measurement (i.e., the baseline data).
- **CSI Pre-Processing Module:** If the target is located in FFZ of a specific link, LiFS pre-processes the raw CSI measurements of this link with the scheme introduced in Section 5; otherwise, LiFS uses the scheme proposed in FILA [39] to pre-process the measurements.
- **Target Localization Module:** For each link, LiFS formulates a PFM equation with the pre-processed CSI measurement. By solving a set of PFM equations formulated for all the links, LiFS can estimate the target location accurately as described in Section 6.

In the next few sections, we first introduce some background information and then provide the technical details.

4. BACKGROUND

4.1 Channel State Information Measurement

Most modern digital radios use OFDM communication and transmit signals across orthogonal subcarriers at different frequencies [23, 26]. Each transmitted symbol $X(f)$ is modulated on a subcarrier index f, and the received symbol $Y(f)$ depends on the wireless channel $H(f)$:

$$Y(f) = H(f) \times X(f). \quad (1)$$

The channel matrix $\mathbf{H} = \{H(f)\}_{f=1,\cdots,K}$ is called the *channel state information*, where K is the number of subcarriers. Each $H(f) = |h_f| e^{\mathbf{J}\cdot\theta_f}$ is a complex value depicting the changes of the amplitude $|h_f|$ and the phase θ_f between transmitter and receiver at subcarrier f, where $\mathbf{J}$ is the imaginary unit. That is to say, the CSI amplitude measures the power fading of the Wi-Fi link between the transmitter and the receiver. For each transmission, a group of CSI measurements on $K = 30$ subcarriers are exported by leveraging a COTS Intel 5300 NIC with a public driver [9, 8].

4.2 Power Fading Model

To localize a target, we need to understand the effect of a target's location on the CSI measurement. Let λ denote the wavelength of the wireless signal and we use the location vector $C = [x, y]$ to describe the 2D coordinate. Then, the coordinates of the transmitter i, receiver j and the target are referred to as C_i, C_j and C_t, respectively. Then the wireless link ℓ_{ij} between transmitter i and receiver j has a length of $d_{ij} = \sqrt{(C_i - C_j)^T (C_i - C_j)}$. Similarly, we can calculate d_{it} and d_{jt}, which are the distances from the target

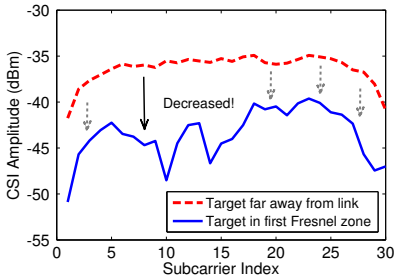

Figure 3: CSI measurements in an outdoor open space with and without a target located in FFZ.

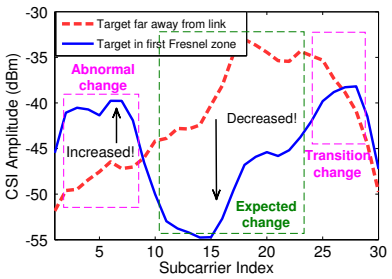

Figure 4: CSI measurements in a typical office room with and without a target located in FFZ.

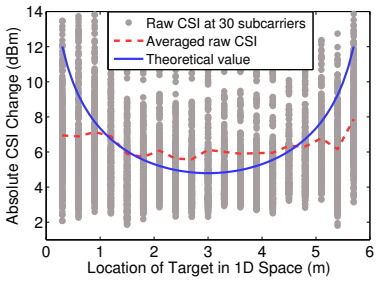

Figure 5: CSI change measurements of the raw data at 30 subcarriers when a target is located at different locations.

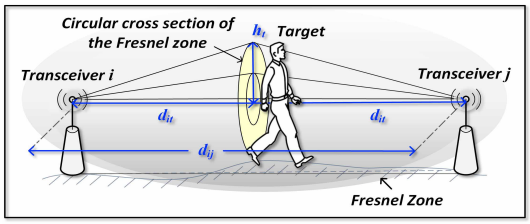

Figure 6: Power fading model.

to the transmitter i and the receiver j. According to wireless communication principles [21], the power fading between the two transceivers is mainly related to the *propagation fading*, *diffraction fading* and *target absorption fading*.

Propagation fading: Propagation fading L_{ij} specifies the attenuation due to propagation of a distance d_{ij} between the transmitter i and the receiver j [21] as follows in dBm:

$$L_{ij} = 10\log[\lambda^2/(16\pi^2 d_{ij}^2)]. \quad (2)$$

Diffraction fading: Diffraction fading D_{ijt} specifies the attenuation due to a target located in the First Fresnel Zone (FFZ) of link ℓ_{ij} [21]. A Fresnel zone is an ellipsoid whose foci are the transmitter and the receiver, as shown in Fig. 6. The radius of the circular cross section of the FFZ is given by $r_1 = \sqrt{(\lambda \cdot d_{it} \cdot d_{jt})/d_{ij}}$. The diffraction fading is significant when a target is located within the FFZ; while the diffraction fading is very small when the target is far away from the FFZ [21]. D_{ijt} is a function of the distances from the target to transmitter i and receiver j, which is given by:

$$D_{ijt} = 20\log\left(\frac{\sqrt{2}}{2} \cdot \left|\int_v^{\infty} \exp(\frac{-\mathbf{J} \cdot \pi z^2}{2})dz\right|\right), \quad (3)$$

where $v = h_t\sqrt{2(d_{it}+d_{jt})/(\lambda \cdot d_{it} \cdot d_{jt})}$ determines the volumes of the diffraction fading, and h_t is the target's effective height. h_t is defined as the distance from the highest point of the target to the wireless link.

Equation (3) shows that we need to know the effective height in order to localize the target. Fig. 6 describes an ideal example where the heights of the two transceivers are the same. In this case, the effective height is a constant wherever the target is located. However, the heights of transceivers will be different in reality. As a result, the effective height is always changing when a target is located at different locations. Since the target location is an unknown, it is impossible to predict the effective height beforehand. We present our solution to handle this "changing effective height" problem in Section 6.

Target absorption fading: When a target is located exactly on the LoS path, a link suffers large extra signal attenuation absorbed by the target, which is denoted as A_t ($A_t < 0$) and is dependent on the target.

Putting things together, when a target is located in the monitoring area, the power fading between the transmitter i and the receiver j, i.e., the CSI amplitude[4] measurement R_{ij}, is expressed as below in dBm:

$$R_{ij} = \begin{cases} L_{ij} + D_{ijt} + A_t + \eta, \ LoS, & (4) \\ L_{ij} + D_{ijt} + \eta, \ NLoS \ but \ still \ in \ FFZ, & (5) \\ L_{ij} + \eta, \quad outside \ of \ FFZ, & (6) \end{cases}$$

where η is the measurement noise. "NLoS but still in FFZ" in Eqn. (5) means that the target is not on the LoS path but still located in FFZ. We refer Eqn. (4), Eqn. (5) and Eqn. (6) as the power fading model and rewrite them as R_{ij}=$PFM(C_i, C_j, C_t, h_t)$. For simplicity, we use "CSI" to represent "CSI amplitude" in the rest of this paper.

5. PRE-PROCESSING CSI MEASUREMENT

For a given deployment setup, the power fading model shows that the CSI change is only related to a target's location and the effective height when the target is located inside the FFZ. However, strong multipath reflections and environmental noise [40, 47] may also affect the CSI change. We would like to filter out those subcarriers greatly affected by multipath and noise, thus only retrieving the CSI changes on the "clean" subcarriers for our location estimate.

5.1 CSI Change in Multipath Environment

To understand the CSI changes in rich multipath environment, we conduct experiments in both an outdoor open space and a typical indoor office room. In each environment, an AP acts as the transmitter and a laptop equipped with Intel 5300 NIC is employed as the receiver. We set the distance between the transmitter and the receiver as 6 m and place the two transceivers at the same height in order to eliminate the impact of height difference. In each environment, we collect two sets of CSI measurements when a target is located inside and outside the FFZ, and the results are shown in Fig. 3 and Fig. 4, respectively.

Fig. 3 illustrates that the CSI amplitudes of all the subcarriers are decreased in the open space environment when a target is located in the FFZ, which is consistent with the

[4]Note that the Intel 5300 NIC reports the CSI amplitude in voltage space [8]. We convert the amplitude of CSI $|h|$ into R with the unit of dBm as: $R = 20\log(|\mathrm{h}|/1000)$.

diffraction theory [21]. However, in the indoor office environment, the situation is more complicated. Fig. 4 displays that the CSI amplitudes of some subcarriers are increased (e.g., the 5th subcarrier) or remain unchanged (e.g., the 9th subcarrier), which are obviously inconsistent with the diffraction theory. Thus, if we apply the power fading model directly on the raw CSI measurements, these inconsistencies will result in large localization errors. For example, Fig. 5 shows the CSI changes of all subcarriers when we let a target move along the LoS path from the transmitter to the receiver. For evaluation purposes, we also plot the theoretical CSI values in Fig. 5 based on the diffraction theory in Eqn. (3). We can see that the variations of the raw CSI change measurements are quite large, and the averaged values do not match the theoretical curve well.

The CSI changes at all subcarriers in an indoor environment can be categorized into three groups which we term them as *expected change*, *abnormal change* and *transition change* shown in Fig. 4. The *expected change* has a feature similar to the outdoor open space environment, which is mainly caused by the presence of a target and conforms to the diffraction theory. The *abnormal change* has an opposite effect to the *expected change*, i.e., the CSI amplitude is increased rather than decreased. This *abnormal change* is caused by constructive multipath propagations in the indoor environment. The *transition change* is the "transition zone" between the *expected change* and the *abnormal change*.

5.2 Pre-Processing Scheme for CSI

The intuition of the pre-processing scheme is that different subcarriers are experiencing frequency-selective fading [10]. Thus, not all subcarriers are affected equally by the multipath as depicted in Fig. 4. Our objective is to remove those subcarriers greatly affected by multipath because the CSIs on these subcarriers do not fit the theoretical model. To filter out these *dirty subcarriers* with abnormal CSI changes, our first step stems from the "power increase" observation at some subcarriers. Specifically, when the CSI amplitude of the k-th subcarrier is increased instead of decreased, we know the subcarrier is affected by multipaths and the CSI measurement at this subcarrier should be filtered out. Unfortunately, it is not easy to filter out the *transition part* since it may also exhibit the "power decrease" feature. To address this issue, we adopt a threshold to filter out the subcarriers in the transition part based on whether the power decrease is large enough. Specifically, if a target is not located on the LoS path, the threshold δ_{eff} is defined as the averaged standard deviation over all the K subcarriers:

$$\delta_{eff} = \frac{1}{K}\sum_{k=1}^{K}\frac{f_k}{f_0}\times\delta_k, \tag{7}$$

where f_0 is the central frequency, f_k is the frequency of k-th subcarrier, and δ_k is the standard deviation of the amplitudes of baseline CSI measurements on k-th subcarrier when no target is present. A large number of baseline CSI readings is helpful for an accurate δ_k estimation. However, it incurs a high latency. In our experiments, we find 100 CSI readings are good enough and it takes 10 s when we employ beacons with 100 ms interval. Note that the different weighting factors $\frac{f_k}{f_0}$ is based on the fact that radio propagation is frequency-dependent [39]. If a target is located on the LoS path, the threshold δ_{eff} should be added with the absolute signal attenuation $|A_t|$ caused by the target. To identify whether a target is located on the LoS path, the key observations are (i) $|A_t|$ is usually within the range of 4–9 dBm [31, 34, 32] when a human target blocks the LoS path, and (ii) the noise is usually within 1–3 dBm [30, 48]. Thus, a target is more likely located on the LoS path if the averaged CSI change of all subcarriers is larger than 5 dBm. Unless specifically mentioned, we denote δ_{eff} as the threshold for simplicity in the rest of this paper.

Let $\mathbf{F} = \{F_1, F_2, \cdots, F_K\}$ be the CSI measurements when a target is inside the FFZ of a link, and $\mathbf{O} = \{O_1, O_2, \cdots, O_K\}$ be the baseline CSI measurement acquired when we make sure there is no target present in the monitoring area. I is a set of subcarrier indices in which the CSI amplitude decrease is larger than the threshold δ_{eff}, i.e., $I = \{j : F_j - O_j > \delta_{eff}, 1 \le j \le K\}$. When a target appears, the *effective CSI* value CSI_{eff} and the *effective CSI change* value ΔCSI_{eff} are calculated as:

$$CSI_{eff} = \frac{1}{|I|}\sum_{j\in I}\frac{f_j}{f_0}\times F_j, \tag{8}$$

$$\Delta CSI_{eff} = \frac{1}{|I|}\sum_{j\in I}\frac{f_j}{f_0}\times (F_j - O_j). \tag{9}$$

We emphasize that the effective CSI CSI_{eff} is the desirable output of the pre-processing scheme. If a target is located on the LoS path, CSI_{eff} should conform to Eqn. (4), otherwise it should conform to Eqn. (5). The effective CSI change ΔCSI_{eff} should conform to the diffraction fading D in Eqn. (3). Obviously, if ΔCSI_{eff} matches the model-calculated D well, the power fading model can be applied to estimate a target's location accurately. Note that we have CSI from 30 subcarriers and as long as a few of them fall in the *clean* category, it is enough for our localization purposes. In the future, we will improve the accuracy of selecting the clean subcarriers with the help of phase information. For example, multiple adjacent subcarriers should exhibit a linear phase change if these subcarriers are clean. However, the phase information obtained from COTS Wi-Fi devices is very noisy [41] and can not be applied directly.

5.3 CSI Pre-Processing Scheme Verification

Under the same deployment setup described in Section 5.1, we conduct experiments in three different environments, i.e., a library, an office and an indoor empty hall corresponding to high, medium and low multipath scenarios. Due to space limitations, we only show the experimental environment and the deployment setup of the indoor office in Fig. 8. In all three environments, we set the distance between the laptop and the AP to be 6 m. The following three claims validate the effectiveness of our pre-processing scheme.

Claim 1. *The CSI pre-processing scheme removes the subcarriers which are greatly affected by multipath and preserves those relatively "clean" CSI measurements which are not affected by multipath much.*

To verify the effectiveness of our scheme in identifying the "clean" subcarriers, we acquire ground truth with the help of CSI measurements in an outdoor open space which has very little multipath. We make sure the link length and the relative target location are the same in both outdoor open space and indoor environment. First, in the outdoor open space, we obtain a relatively stable and constant CSI change at all the subcarriers because of little multipath. Then, in

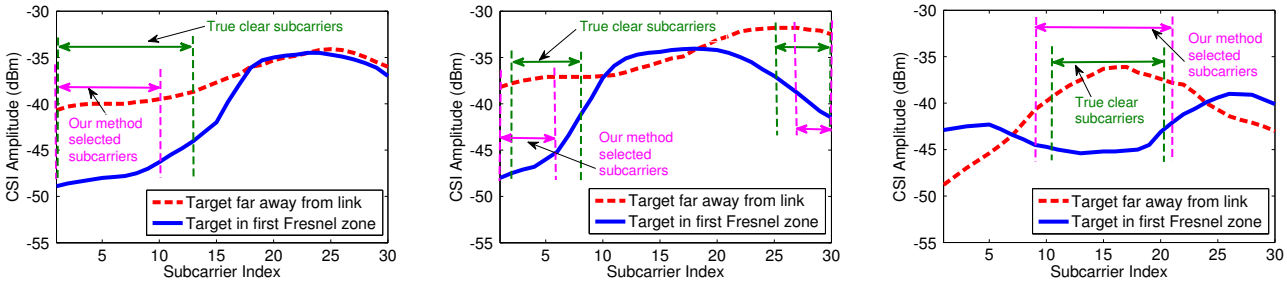

(a) Target stands at LoS "location 1". (b) Target stands at LoS "location 2". (c) Target stands at NLoS "location 3".

Figure 7: CSI amplitudes of all the subcarriers when a target is located inside the FFZ at three different locations.

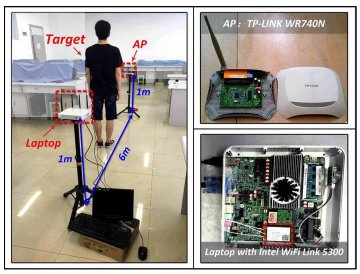

Figure 8: Experimental environment and deployment setup.

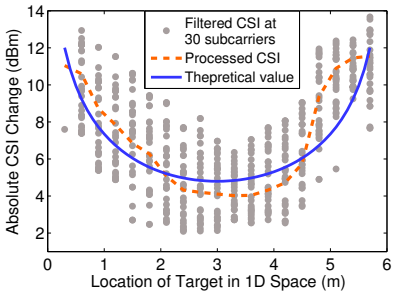

Figure 9: CSI change measurements after pre-processing.

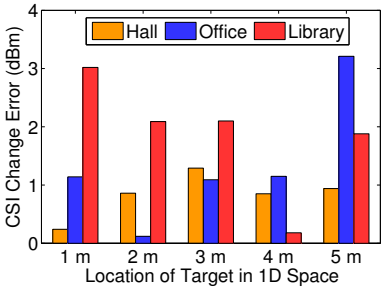

Figure 10: Absolute CSI change error under three different environments.

the indoor environment, we identify the subcarriers with CSI changes close to the stable change in the outdoor open space as the "clean" subcarriers.

Fig. 7(a)–(c) show the CSI amplitudes of all the subcarriers when a human target is located inside the FFZ at three different locations in the office. The corresponding CSI changes in an open space are acquired from Fig. 3. The mean and standard deviation of the CSI changes over all the subcarriers in Fig. 3 are 7.25 dBm and 2.02 dBm, respectively. Due to the environmental and hardware noises, we take subcarriers whose CSI changes are within 7.25-2.02 dBm and 7.25+2.02 dBm as the ground truth "clean" subcarriers. Our CSI pre-processing scheme chooses the subcarriers whose CSI decreases are larger than the threshold δ_{eff}. Fig. 7(a)–(b) show the results when the target is located on the LoS path at two different locations, and Fig. 7(c) shows the results when a target is located on the NLoS path but still in FFZ. In this experiment, the averaged standard deviation over all subcarriers is 2.82 dBm and the minimum empirical absolute signal attenuation $|A_t|$ caused by the target is 4 dBm. Thus, the threshold δ_{eff} is 6.82=2.82+4 dBm in Fig. 7(a)–(b), and 2.82 dBm in Fig. 7(c). Based on these thresholds, the results of Fig. 7(a)–(c) show that the subcarriers selected by our pre-processing scheme match the ground truth "clean" subcarriers quite well. Note that, multipath may also cause a signal power decrease on some subcarriers. However, it's challenging to identify these subcarriers as the attenuations caused by the human body vary a lot. So we only remove those subcarriers definitely affected by multipaths and still keep the rest. Moreover, we input the averaged CSI changes of all selected subcarriers into the model thus the few wrongly selected subcarriers have a small impact in the localization performance.

To summarize, our pre-processing scheme is able to preserve those relatively "clean" CSI measurements which are not affected by multipath much. We only show the results in the office here as the results from the other two environments have a similar trend.

Note that the method to obtain ground truth "clean" subcarriers for verification can not be applied to identify the "clean" subcarriers in localization experiments because it requires the link length and target location as the input which are not available. On the other hand, the proposed pre-processing method does not need to know this information.

Claim 2. *The pre-processed CSI change measurement matches the diffraction-model-calculated value well.*

Fig. 9 shows the pre-processed CSI measurements when a target moves along the LoS path between transmitter and receiver as mentioned in Section 5.1. For each location, we acquire the pre-processed CSI change ΔCSI_{eff} based on Eqn. (9). Compared with the raw CSI measurements which behave quite randomly as shown in Fig. 5, the pre-processed CSI changes are relatively stable and match the model-calculated values well in Fig. 9. We also evaluate our pre-processing scheme in different multipath environments. Fig. 10 shows the CSI change errors between the pre-processed CSI changes and the model-calculated values in hall, office room and library environments. Most errors are below 1.5 dBm which is smaller than the noise value which is 2.82 dBm. These results imply that our pre-processing scheme can effectively retrieve those clean subcarriers which conform to the diffraction model, and thus ensure a high localization accuracy even in a rich multipath environment.

Claim 3. *The pre-processed CSI is a fine-grained spatial indicator.*

A fine-grained spatial indicator should have the capability to distinguish a target's small movements. The distinguishing capability is reflected in the dissimilarities of the two

CSI measurements. A CSI measurement is a K-dimensional vector whose elements are from K subcarriers rather than a single value. Following Wang *et al.* [33], we use the dynamic time warping (DTW) distance [24] to calculate the dissimilarities of two CSI measurements when a target is at different locations. The detailed DTW distance calculation is presented in Appendix.

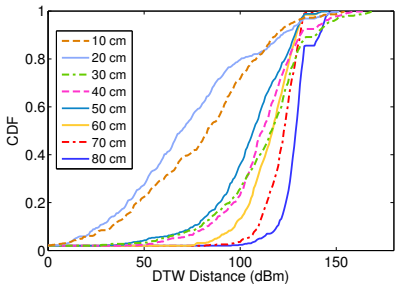

Figure 11: DTW distances of the pre-processed CSI.

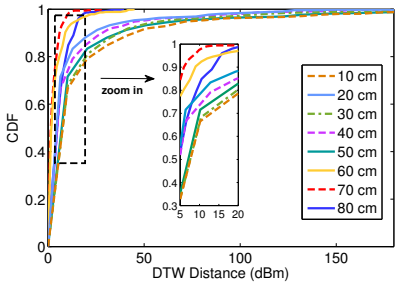

Figure 12: DTW distances of the raw CSI.

To understand the spatial resolution and the discrimination capability of the pre-processed CSI measurements, we have a person move from a reference position with a step size of 10 cm and compute their respective DTW distance with the reference position over 100 measurements. Fig. 11 shows that the median DTW distance of the pre-processed CSI measurements is large even when the distance is 10 cm. Note that it's possible two different pairs of CSIs can have the same DTW distance. However, the probability is very low since the CSI changes are relatively random due to the multipath indoors. Even if two pairs of CSIs have the same DTW distance, we can utilize the DTW distances at nearby locations to differentiate them since it is not likely the DTW distance at nearby locations are same again.

6. SYSTEM DESIGN

6.1 Basic Idea of LiFS

Suppose there are N APs, M clients and one target, which are randomly located in a 2D monitoring area. The number of wireless links between APs and clients is MN. We can also measure a number of $N(N-1)/2$ wireless links between all the APs.[5] Thus, based on the power fading model introduced in Section 4, we can establish a number of $MN + N(N-1)/2$ equations to restrict the location of the target. The locations of APs are fixed and known in reality.

[5]Note that we do not consider the links between clients as we only assume access to CSI information from the APs.

Both the target and each of the M clients have two unknown parameters, namely their $[x, y]$ coordinates in the 2D space. As mentioned in Section 4, a target's effective height keeps changing and it is impossible to predict this change. Thus, we also treat the effective height as an unknown. Then, the total number of unknowns is no larger than $2M + 3$, since the locations of some clients are known. Note that the number of equations $MN + N(N-1)/2$ grows in a quadratic fashion, while $2M + 3$ grows linearly. This suggests that given enough number of clients and APs ($N > 3$), such that $MN + N(N-1)/2 > 2M + 3$, there will be enough constraints to determine all the unknown locations of both the target and the unknown clients.

6.2 Location Determination via Optimization

After modelling a set of power fading model equations, LiFS needs to solve these equations. There are several approaches to solve a set of over-determined equations such as inverting the power fading model equations directly or applying the least squares method. However, these approaches are not efficient due to the complex non-linear Fresnel integrations in the power fading model.

In this work, we solve these equations by attempting to minimize the mean absolute error between the processed CSI data and the power fading model calculated CSI value. More specifically, let $y_{ij} \in Y$ be the pre-processed CSI measurement of the link ℓ_{ij} $(1 \le i \le N,\ 1 \le j \le M)$. Then our objective function J is given by:

$$J = \min \frac{1}{|Y|} \sum |y_{ij} - PFM(C_i, C_j, C_t, h_t)|, \qquad (10)$$

where, C_i, C_j and C_t are the locations of APs, clients and the target respectively, and h_t is the target's effective height. We use the wavelength at the center frequency f_0 for calculating the CSI values in power fading model.

LiFS pre-processes y_{ij} with two different schemes. If the target is located in the FFZ of a link, LiFS pre-processes the raw CSI measurement of this link with the scheme introduced in Section 5. Otherwise, LiFS uses the scheme proposed in FILA [39], which is given by:

$$CSI_{eff} = \frac{1}{K} \sum_{k=1}^{K} \frac{f_k}{f_0} O_k, \qquad (11)$$

where O_k is the CSI measurement of k-th subcarrier, f_0 is the central frequency, f_k is the frequency of k-th subcarrier and K is the total number of subcarriers.

The principle of selecting pre-processing schemes will be introduced later at the end of this subsection. Now, we focus on how to solve Eqn. (10). It is noted that J is a non-linear function due to the Fresnel integration. In this case, the gradient descent (GD) algorithm [4] and the genetic algorithm (GA) algorithm [18] are usually employed since they are more efficient than the traditional method such as the least squares method. The GD algorithm starting from an initial guess is able to find the closest local minimum. However, the GD algorithm may fail to find a good solution when the number of local minima in J is large. While the GA algorithm can search the solution space more efficiently, it sometimes misses local minima that might provide a reasonably good solution. To gain the benefits of both approaches, motivated by Chintalapudi *et. al.* [7], we use a GA and GD hybrid method to obtain the solutions of all unknowns, i.e., C_j, C_t and h_t to be solved. In each iteration, GA starts pick-

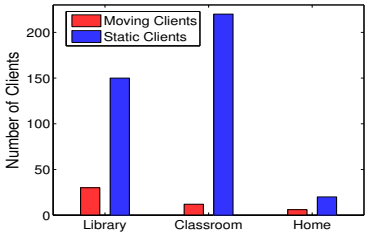

Figure 13: Average number of moving and static clients in different environments.

(a) Library environment.

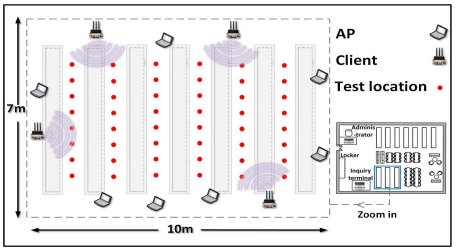

(b) Testbed floorplan with 48 test locations.

Figure 14: Experimental environment and floorplan of a library (strong NLoS).

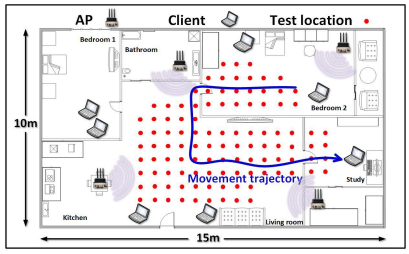

Figure 15: Testbed floorplan of a home with 107 test locations.

(a) Classroom environment.

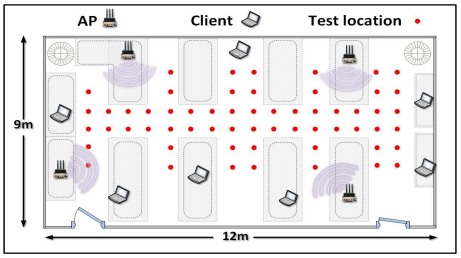

(b) Testbed floorplan with 57 test locations.

Figure 16: Experimental environment and floorplan of a classroom (strong LoS).

ing a set of solutions (initiates all the unknowns) and then refines the solutions via the GD algorithm. Each solution is then evaluated by computing the J value.

Which power fading model formulas should we choose to form the equations? Since the equations in power fading model are based on the location where the target is located, i.e., LoS, NLoS but still in FFZ, and outside of FFZ. Thus, the power fading model equations are formed with a rough estimation of the target's location. Note that the CSI change is negligible when a target is outside of FFZ while the CSI change is large when a target is on LoS path. Thus, LiFS can estimate the location range of a target roughly based on just the effective CSI changes as below:

$$\begin{cases} |\Delta CSI_{eff}| > |A_t| \Rightarrow \textit{LoS (in FFZ)}, \\ \delta_{eff} < |\Delta CSI_{eff}| \leq |A_t| \Rightarrow \textit{NLoS but still in FFZ}, \\ |\Delta CSI_{eff}| \leq \delta_{eff} \Rightarrow \textit{outside of FFZ}. \end{cases} \tag{12}$$

where δ_{eff} ($\delta_{eff} > 0$) is the threshold when no target is present and δ_{eff} can be calculated based on Eqn. (7), and A_t is the target absorption attenuation when the target is located on LoS path. Accordingly, the pre-processing scheme is chosen as follows: (i) The raw CSI values are pre-processed by our scheme in Section 5.2 if the target is located in FFZ; (ii) The raw CSI values are pre-processed by the method proposed in [39] if the target is outside of FFZ.

The signal attenuation A_t is dependent on the target so an overweight man may cause a larger signal attenuation than a slim man. To deal with this problem, LiFS takes A_t as an unknown in addition to all the other unknowns. The good thing is that the number of unknowns is usually much smaller than the equations, so one added unknown will not affect the performance of LiFS. To estimate A_t, we first pick an initial value for A_t based on the empirical knowledge. $|A_t|$ is usually within 4–9 dBm [32, 34, 31]. Even if there is a large error in the initial guess for A_t, the optimization scheme is able to reduce the error to a small value after several iterations. For example, in our experiments, the variations of the estimated A_t are no larger than 2 dBm after 3–5 optimization iterations.

6.3 Coping with Client Mobility

In practice, most clients are mobiles and laptops whose locations may change sometimes. However, it is not likely for all users to move their devices simultaneously and frequently. We record the number of moving and static clients in two days across three different environments. We divide two days into 288 10-minute window pieces. Fig. 13 shows the average number of moving and static clients across the 288 slots. We can see clearly that most of the time the majority of clients are static. By observing the CSI variations of multiple APs, we can filter out the CSI data from moving clients and only keep the data from the static clients. So for a specific client, if multiple APs observe large CSI variations simultaneously, then this client is likely to be moving and will not be included for localization.

7. IMPLEMENTATION

Experimental environments: To verify the effectiveness of LiFS, we conduct experiments in three different environments. The first is a typical home environment with a size of 10 m × 15 m. It has furniture and obstacles in the form of concrete walls and glass/metal doors. Due to privacy concerns, we only present the testbed floorplan in Fig. 15. The second environment is part of a library with a size of 7 m × 10 m. The library has many shelves as shown in Fig. 14. The shelves have a height of 2.5 m and are made of metal and wood, resulting in a rich multipath and strong NLoS scenario. The third environment is an indoor classroom with a size of 9 m × 12 m. The classroom has some empty desks, resulting in a strong LoS scenario as shown in Fig. 16. In each environment, the test locations are 0.6 m separated from each other, and a person with a height of 1.72 m acts as the target.

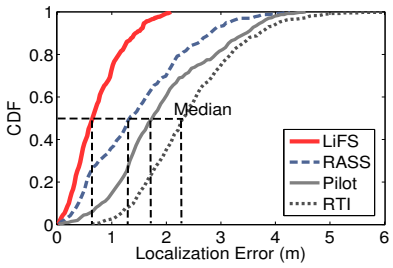

Figure 17: CDF plot of the localization errors in home.

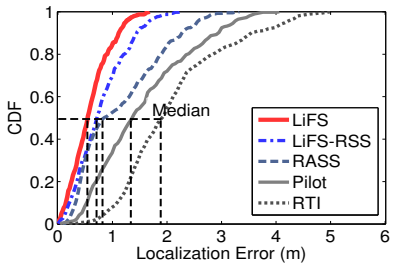

Figure 18: CDF plot of the localization errors in classroom (strong LoS).

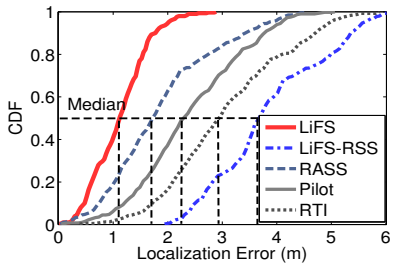

Figure 19: CDF plot of the localization errors in library (strong NLoS).

Hardware configuration: In each environment, we deploy 11 laptops, each of them equipped with an Intel 5300 NIC. Four of the 11 laptops are modified to act as APs with the "hostapd" tool in [17] and the remaining 7 laptops act as clients. For all environments, the locations of APs, clients together with the test points are marked in Fig. 14(b), Fig. 15 and Fig. 16(b), respectively. Each AP probes the other 3 APs and all the clients every 100 ms (a typical beacon transmission interval) to obtain CSI. To reduce the probing overhead, we can also use link layer NULL frames to probe a client. Moreover, LiFS works with any packet, so it can reduce the amount of deliberately-transmitted packets by employing the transmissions from ongoing data communication and the beacons from APs. Note that LiFS does not require all APs and clients to be on the same channel. A target can affect two links on different channels and the power fading information from both links can be employed for localization. A desktop with 3.6 GHz CPU (Intel i7-4790) and 8 GB memory is employed as the server to collect CSI measurements through wired connections and runs our localization algorithm.

Default deployment setup: In reality, the locations of APs and some clients are fixed and known. Thus, we assume the locations of all the 4 APs and one of the 7 clients are known in our experiments. Usually, most clients (such as laptops or mobiles) rest on a table or are held in the hand, so we set the heights of clients as 1.2 m off the ground. The heights of APs vary a lot. Some users like to place the APs on the wall which is higher than a table, while others still place the APs on the table. Thus, we place two APs at a height of 1.7 m above the ground and the rest two APs on the table with a height of 1.2 m. Note that, for each Intel 5300 NIC, we only choose one antenna to receive or transmit packets. When we evaluate the impact of the number of clients in Section 8.3.1, we employ more antennas and treat each antenna as an independent client. Unless specifically mentioned, we use the default setup introduced here for performance evaluation in the rest of this paper.

Experimental methodology: LiFS has two phases. First is the baseline data acquisition when no target is present. Each pair of transceivers (consisted of an AP and a client) records 10 packets and forwards the packets to the server. Second is the localization phase. When a target moves into the monitoring area, each pair records 10 packets and also forwards the packets to the server. At the server side, LiFS pre-processes the CSI data and estimates the target's location by solving the power fading model equations. In order to eliminate the random errors, we run both LiFS and other localization schemes 40 times at each test location.

8. PERFORMANCE EVALUATION

8.1 Comparison and Metric

We compare LiFS with three other schemes in real indoor environments described in Section 7.

- **Pilot:** Pilot [40] is a state-of-the-art CSI-based device-free localization scheme utilizing the CSI correlations of all subcarriers as fingerprints. Pilot uses the kernel density-based maximum a posteriori probability (MAP) algorithm to localize a target. We find that Pilot performs the best when the kernel bandwidth is 3, and we use this setting in our experiments as well.
- **RASS:** RASS [49] is a power-based scheme which utilizes the RSS change, i.e., the averaged CSI amplitude changes over all subcarriers as fingerprints. RASS uses the support vector regression algorithm to localize a target. For a fair comparison, we use pre-processed CSI change measurements as the input for RASS and employ the "LIBSVM" tool [15] used in RASS to localize a target.
- **RTI:** RTI [38] does not need offline training effort, which has the similar advantage as LiFS. RTI requires the prior knowledge of all the transceivers' locations. For a fair comparison, we employ the scheme proposed in the well-known EZ [7] system to localize the unknown transceivers.

Performance metric. Most human targets have a width of no larger than 40 cm. To calculate the localization error, we can not treat human target as a point. Thus, we consider there is no localization error as long as the estimation is within 20 cm range centred on the true location. Otherwise, the error is calculated as the minimum distance between the estimated location and this range area.

8.2 Overall Localization Accuracy

We show the overall performance comparisons in three different environments, i.e., a home , an open classroom (strong LoS) and a library (strong NLoS).

8.2.1 Localization accuracy in home environment

We have the test subject go through all 107 test locations. Fig. 17 depicts the cumulative distribution function (CDF) plot of localization errors obtained for all the four schemes. It shows that LiFS performs the best with median and 80-percentile errors as small as 0.7 m and 1.2 m. RASS, Pilot and RTI yield large median errors of 1.4 m, 1.8 m and 2.4 m.

The poor performance of RTI is due to the fact that RTI needs precise locations of all the transceivers (i.e., APs and clients). The unknown transceivers' location errors caused

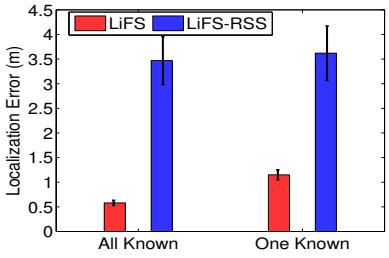

Figure 20: Localization errors with some clients' locations known.

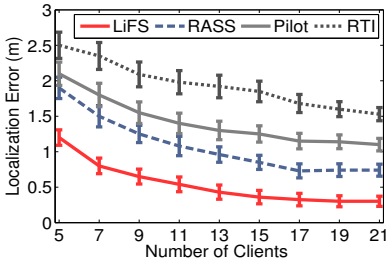

Figure 21: Impact of the number of clients.

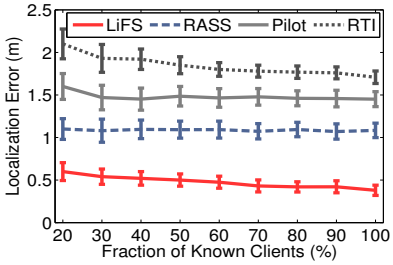

Figure 22: Impact of the fraction of known location clients.

by EZ would decrease the localization accuracy of RTI. Unlike RTI, LiFS can localize the target accurately without requiring to know all the transceivers' locations.

The performance of RASS and Pilot is not as good as LiFS since the CSI measurements vary over time [9]. Thus, the online measurements will not match the fingerprints in the database, resulting in large errors. Unlike RASS and Pilot, LiFS does not rely on manually-collected fingerprints. By modelling the pre-processed CSI measurements with the power fading model equations, LiFS has sufficient restrictions to localize the target accurately.

Compared with Pilot, the superiority of RASS stems from our CSI pre-processing scheme. The space distance of the pre-processed CSI data is larger than the raw CSI data as validated in Section 5.3. As a result, RASS with the pre-processed CSI data outperforms Pilot with the raw CSI data.

8.2.2 *Evaluation in LoS and NLoS scenarios*

In this subsection, we answer the following two questions: First, what is the localization accuracy of LiFS in LoS and NLoS scenarios? Second, compared with RSS, how much accuracy has been improved by the pre-processed CSI? To answer the questions, we choose the open classroom environment (Fig. 16) and the library environment (Fig. 14).

Fig. 18 and Fig. 19 show the localization errors for all the four schemes in strong LoS and strong NLoS scenarios. All the schemes perform better in strong LoS scenario. Compared with LoS scenario, the median localization errors of LiFS, RASS, Pilot and RTI degrade by about 2×, 2.3×, 1.7× and 1.5× in NLoS, respectively. Overall, LiFS achieves 1.6×, 2.8× and 3.8× higher accuracies than RASS, Pilot and RTI in LoS, and 1.6×, 2.2× and 2.7× in NLoS scenario.

The decrease in localization accuracy of LiFS in NLoS scenario is mainly due to the errors in clients' location estimations. As shown in Fig. 20, when all the 7 clients' locations are known, LiFS's mean localization error in NLoS is about 0.6 m, which is very close to the accuracy (i.e., 0.5 m) in LoS. It implies that LiFS in NLoS can perform as well as in LoS if all clients' locations are estimated accurately.

The localization errors of LiFS using RSS in LoS and NLoS scenarios are also shown in Fig. 18 and Fig. 19. The localization accuracy of LiFS using RSS is comparable to employing the pre-processed CSI in LoS. The reason is that the RSS values match the model relatively well in LoS because of little and weak multipath. In contrast, when there is rich multipath in the NLoS scenario, only a few subcarriers' CSI amplitudes match the proposed model. RSS is an averaged "CSI amplitude" over all subcarriers [9, 8]. Consequently, the RSS values do not match the model, and LiFS with RSS suffers large errors in the NLoS scenario.

8.3 Performance under Different Parameters

In this subsection, we evaluate LiFS' performance under varying parameters in the home environment shown in Fig. 15 with both LoS and NLoS Wi-Fi links.

8.3.1 *Impact of the number of clients*

To examine the impact of the number of clients on LiFS' performance, we increase the number of clients from 5 to 21 with a step size of 2, while only one client's location is considered as known. As illustrated in Fig. 21, it is apparent that the average localization errors of all the schemes become smaller with more clients deployed. The intuition is that, with more clients, LiFS (including other systems) has more constraints on a target's location. Because of the same reason as we explained in Section 8.2, LiFS always outperforms the other three schemes.

8.3.2 *Impact of the fraction of known clients*

If more clients' locations become available, we would expect LiFS' performance to be improved. To evaluate this, we employ 10 clients and increase the fraction of clients with known locations from 20% to 100% with a step size of 10%. Fig. 22 shows that the localization errors of LiFS and RTI decrease with the increased fraction of known-location clients. We attribute the improvement to the following reasons. The localization accuracy of LiFS and RTI is related to the location precision of the clients as discussed in Section 4. With more clients knowing their locations, less error would be added into the target's location estimation. For RASS and Pilot, their localization errors are almost unchanged with the increase of the number of known clients. Since RASS and Pilot are "training and matching" schemes, which do not rely on the clients' locations [49, 40].

8.3.3 *Impact of AP-client height difference*

In reality, APs and most clients are not placed at the same height. We seek to study whether this height difference would cause large location errors. To do so, we place all the clients on several desks which are 1.2 m off the ground. Then, we simultaneously increase the heights of all APs from 1.2 m to 2.4 m with a step size of 0.4 m. Fig. 23 shows the experimental results under different height differences. The right subgraph shows the detection rate and the left subgraph shows the localization error. The detection rate is defined as the number of locations can be localized divided by the total number of test locations. Fig. 23 shows that the detection rate is decreased with the increase of height difference. The reason is that when an AP is placed higher than a target, the target near to the AP is away from the wireless link formed and thus would not be detected. However, when

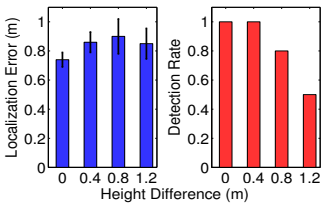

Figure 23: Impact of the AP-client height difference.

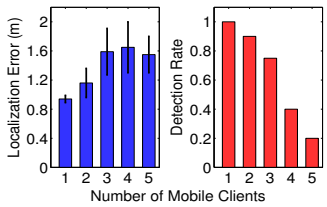

Figure 24: Impact of the movement of clients.

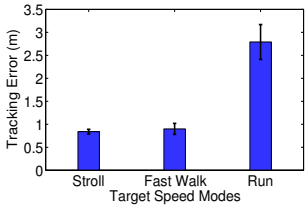

Figure 25: Impact of the target moving speed.

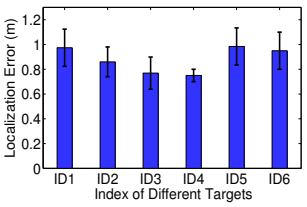

Figure 26: Impact of the target size.

the height difference is below 0.8 m which is commonly seen in reality, the detection rate achieved is no less than 80%.

For a given height difference setting, we only include those test locations at which a target can be detected for localization performance evaluation. Fig. 23 shows that the localization error of LiFS is always less than 1 m no matter what heights of the APs are, since LiFS is able to estimates the unknown height difference together with the target location.

Note that if the APs are mounted on the ceiling, our system may fail in some cases since the wireless links may not be affected by the target. To address this limitation, one possibility is adding some low-height transmitters. Another promising way is utilizing the direct client-to-client communication employed in next generation Wi-Fi technology.

8.3.4 *Impact of the movement of clients*

In practice, most clients are mobiles or laptops. We evaluate the impact of clients' mobility on LiFS' localization accuracy in this section. We let five users randomly move 5 of the 7 clients. Each person picks up one client and keeps the height of the client at 1.2 m. We increase the number of mobile clients from 1 to 5. Fig. 24 shows the experimental results with different numbers of mobile clients.

The right subgraph of Fig. 24 depicts the detection rate. It demonstrates that the detection rate is decreased with more clients moving, since only the wireless links formed by static clients and APs can be utilized for detection and localization as discussed in Section 6.3. It also indicates that as long as the number of static clients is no less than five, which can be easily satisfied in reality, the detection rate is no less than 90%. The left subgraph of Fig. 24 shows that the mean localization errors are always smaller than 1.7 m even with multiple mobile clients.

8.3.5 *Impact of the target moving speed*

We evaluate the tracking performance of LiFS when a target is moving. To do so, we let the test person move from the "Bedroom 2" to "Study" (the movement trajectory is shown in Fig. 15) with three different modes, i.e., stroll (about 1 m/s), fast walk (about 3 m/s) and run (about 5 m/s). For each mode, the target person repeats moving along the trajectory 30 times. Fig. 25 shows the tracking errors under different speeds. The tracking errors of LiFS are always less than 1 m as long as the target is not running.

When a target is running, the CSI changes may vary a lot in a short time. Thus, LiFS can not always get stable CSI changes, causing large errors. Note that in a typical indoor environment, people rarely run. Thus LiFS is suitable for tracking a moving target in most cases.

8.3.6 *Impact of the target size*

In practice, different targets or people are of different sizes, e.g., different weights and heights. We would like to evaluate the impact of target size on LiFS' performance. Under the default experimental setup, we evaluate the performance of LiFS on localizing 6 people with distinct weights and heights. Fig. 26 illustrates the localization errors with different human targets, i.e., ID1 (a child of 40 kg and 140 cm), ID2 (a girl of 48 kg and 165 cm), ID3 (an overweight boy of 85 kg and 170 cm), ID4 (a boy of 65 kg and 175 cm), ID5 (a tall man of 75 kg and 183 cm), ID6 (an overweight tall man of 90 kg and 181 cm). LiFS performs well for all the 6 people with average localization errors between 0.7 m and 1 m. Moreover, the estimated absolute signal attenuations $|A_t|$ for human target ID1–ID6 are 6.5 dBm, 7.1 dBm, 7.8 dBm, 7.4 dBm, 7.6 dBm and 8.1 dBm respectively, which do not vary much across different human targets.

8.4 Two-Target Localization

Here, we discuss the performance of LiFS for localizing two targets. The intuition is that a target is not able to affect all the wireless links simultaneously. When two targets are located sparsely, each target will affect a disjoint subset of links and thus can be separated and individually located. However, when many targets exist or two targets are very close to each other, it's still challenging to accurately localize each of them.

We conduct experiments in the "Living room" of the home setting (Fig. 15) with a size of 7 m $\times$ 6 m. Two persons with heights of 171 cm and 173 cm act as the targets. We let one target move from the top left corner to the lower right corner, and the other target move from the lower right corner to the top left corner simultaneously. Fig. 27 shows four snapshot localization results when the two targets are 5.4 m, 3 m, 1.8 m and 0.6 m away from each other. For each snapshot, we collect 30 measurements and the localization results are mapped into the heatmaps, where the red dots represent the estimated locations and the plus signs indicate the ground truths. LiFS is able to localize the two targets when they are located sparsely. However, when the two targets are close to each other, LiFS has difficulties localizing each individual and we leave this challenging problem as our future work.

8.5 System Latency

Solving a set of power fading model equations by the hybrid GA and GD approach can take a few minutes depending on the problem size. However, the running time can be reduced significantly after one round of operation. Once we have obtained all the transceivers' locations, new target's location query can be answered quickly from the second round.

To demonstrate running time cost of LiFS, we increase the number of unknown clients from 0 to 18, and a total number of 21 clients are deployed. Fig. 28 shows the running time results for localizing a single target. When we run

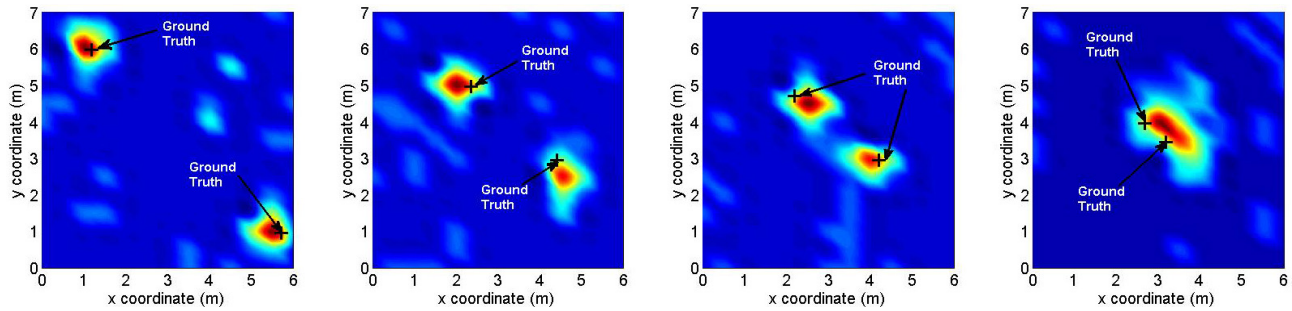

Figure 27: Four snapshot localization results when two targets are 5.4 m, 3 m, 1.8 m and 0.6 m apart, respectively.

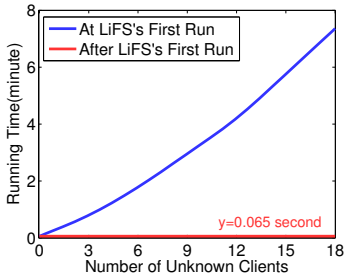

Figure 28: Running time cost of LiFS.

our system at the first time, the running time increases with more unknown clients. However, the running time significantly decreases to 0.065 s after the system's first run, since we only need to estimate the location of the target.

Some clients may move after the system's first run and we still need to find the new locations of the moved clients. However, it is unlikely all the clients move at the same time. LiFS can still localize the target with the static clients and only need to update the locations of a small part of clients.

9. DISCUSSION

Localizability of LiFS: We consider an extreme case here when very limited number of transceivers exist and are not able to cover all the locations in a monitoring area. Then if the target moves into this kind of deadzone not covered by any link, LiFS is not able to localize the target. However, we have three arguments for this extreme case: (i) Usually there are a lot of transceivers in a typical office environment: APs, laptops, mobiles, etc; (ii) A target (person) moves continuously in the physical space, and the target is not likely to jump from one deadzone to another. The target may be within a deadzone only at a particular time. However, the target can still be localized before he/she moves into and after he/she moves out of the deadzone. These location information can be utilized to roughly estimate a target's location when the target is located in the deadzone; (iii) In an office environment, a human target is not likely to be on a table or a bookcase, thus actualy not all the locations need to be covered.

Localization for multiple targets: In this paper, we only present the localization performance of LiFS with two targets. However, we believe LiFS can localize more targets as long as the targets are located sparsely. The most challenging part lies in localizing multiple targets who are close to each other. The multiple target localization accuracy may be improved if our system can first detect the number of targets. This problem is still an open issue [48, 46] and we leave it as the future work.

Localization of a specific target: Our system has the potential to track a specific target. Different human targets may have very different A_t values. By utilizing this A_t as a signature, our system may be able to distinguish different human targets and track a specific target. However, different orientations of the same target may exhibit different A_t values. We leave this interesting problem as the future work.

Impact of Wi-Fi interference: Wi-Fi interference exists in both the pre-obtained CSI baseline measurements and the online measured CSI measurements. The interference will be cancelled out when we calculate the CSI changes. As long as the Wi-Fi interference does not change frequently within a short time period, it will not affect the performance of our system.

10. CONCLUSION

LiFS is a model-based device-free localization system that does not require any explicit pre-deployment effort or exhaustive fingerprint collection. We design, implement and evaluate LiFS against the existing Pilot, RASS and RTI systems which either require the location information of all the transceivers or need an exhaustive fingerprint database. Real-world experiments demonstrate that LiFS outperforms the three state-of-the-art systems in all environments. LiFS also moves one step further on passive multi-target localization which is well known to be challenging.

ACKNOWLEDGMENTS

Thanks the anonymous shepherd and reviewers for their valuable comments. This work is supported in part by National Natural Science Foundation of China under Grants (61272461, 61572219, 61502192, 61572402), and by Fundamental Research Funds for the Central Universities under Grant 2016JCTD118. This research has also received funding from European Research Council under the European Union's Seventh Framework Programme (FP/2007–2013)/ERC Grant Agreement No. 279976. Hongbo Jiang and Xiaojiang Chen are the corresponding authors.

11. REFERENCES

[1] A. Achtzehn, L. Simic, P. Gronerth, and P. Mahonen. A propagation-centric transmitter localization method for deriving the spatial structure of opportunistic wireless networks. In *Proc. IEEE Conference on Wireless On-demand Network Systems and Services (WONS)*, pages 139–146, 2013.

[2] F. Adib, Z. Kabelac, and D. Katabi. Multi-person localization via rf body reflections. In *Proc. USENIX NSDI*, pages 279–292, 2015.

[3] F. Adib and D. Katabi. See through walls with wifi! In *Proc. ACM SIGCOMM*, pages 75–86, 2013.

[4] M. S. Bazaraa, H. D. Sherali, and C. M. Shetty. *Nonlinear programming: theory and algorithms*. John Wiley & Sons.

[5] M. Bocca, O. Kaltiokallio, N. Patwari, and S. Venkatasubramanian. Multiple target tracking with rf sensor networks. *IEEE Trans. on Mobile Computing*, 13(8):1787–1800, 2014.

[6] B. Chen, V. Yenamandra, and K. Srinivasan. Tracking keystrokes using wireless signals. In *Proc. ACM MobiSys*, pages 31–44, 2015.

[7] K. Chintalapudi, A. P. Iyer, and V. N. Padmanabhan. Indoor localization without the pain. In *Proc. ACM MobiCom*, pages 173–184. 2010.

[8] H. Daniel, H. Wenjun, S. Anmol, and W. David. Linux 802.11n csi tool. dhalperi.github.io/linux-80211n-csitool/faq.html.

[9] D. Halperin, W. Hu, A. Sheth, and D. Wetherall. Predictable 802.11 packet delivery from wireless channel measurements. In *Proc. ACM SIGCOMM*, pages 159–170, 2011.

[10] D. Halperin, W. Hu, A. Sheth, and D. Wetherall. Tool release: gathering 802.11 n traces with channel state information. *ACM SIGCOMM Computer Communication Review*, 41(1):53–53, 2011.

[11] P. Jain, J. Manweiler, and R. Roy Choudhury. Overlay: Practical mobile augmented reality. In *Proc. ACM MobiSys*, pages 331–344, 2015.

[12] K. Joshi, D. Bharadia, M. Kotaru, and S. Katti. Wideo: Fine-grained device-free motion tracing using rf backscatter. In *Proc. USENIX NSDI*, pages 189–204, 2015.

[13] J. Kemper and D. Hauschildt. Passive infrared localization with a probability hypothesis density filter. In *Proc. IEEE Workshop on Positioning Navigation and Communication*, pages 68–76, 2010.

[14] M. Kotaru, K. Joshi, D. Bharadia, and S. Katti. Spotfi: Decimeter level localization using wifi. In *Proc. ACM SIGCOMM*, pages 269–282, 2015.

[15] LIBSVM. Library to using svm. www.csie.ntu.edu.tw/cjlin/libsvm/.

[16] H. Ma, C. Zeng, and C. X. Ling. A reliable people counting system via multiple cameras. *ACM Trans. on Intelligent Systems and Technology*, 3(2):31, 2012.

[17] J. Malinen et al. hostapd: Ieee 802.11 ap, ieee 802.1 x. Technical report, WPA/WPA2/EAP/RADIUS Authenticator. online: hostap. epitest. fi/hostapd.

[18] T. Mcconaghy, E. Vladislavleva, and R. Riolo. Genetic programming theory and practice 2010: An introduction. *Gecco Companion Publication Proceedings of Annual Genetic and Evolutionary Computation Conference*, 78(1):3015–3056, 2010.

[19] P. Melgarejo, X. Zhang, P. Ramanathan, and D. Chu. Leveraging directional antenna capabilities for fine-grained gesture recognition. In *Proc. ACM UbiComp*, pages 541–551, 2014.

[20] F. G. Miskelly. Assistive technology in elderly care. *Age and ageing*, 30(6):455–458, 2001.

[21] A. F. Molisch. *Wireless communications*. John Wiley & Sons.

[22] S. Nannuru, Y. Li, Y. Zeng, M. Coates, and B. Yang. Radio-frequency tomography for passive indoor multitarget tracking. *IEEE Trans. on Mobile Computing*, 12(12):2322–2333, 2013.

[23] R. v. Nee and R. Prasad. *OFDM for wireless multimedia communications*. Artech House, Inc.

[24] S. Salvador and P. Chan. Toward accurate dynamic time warping in linear time and space. *Intelligent Data Analysis*, 11(5):561–580, 2007.

[25] L. Shangguan, Z. Li, Z. Yang, M. Li, Y. Liu, and J. Han. Otrack: Towards order tracking for tags in mobile rfid systems. *IEEE Trans. on Parallel and Distributed Systems*, 25(8):2114–2125, 2014.

[26] W. Shen, K. C. Lin, S. Gollakota, and M. Chen. Rate adaptation for 802.11 multiuser mimo networks. *IEEE Trans. on Mobile Computing*, 13(1):35–47, 2014.

[27] Y. Shu, K. G. Shin, T. He, and J. Chen. Last-mile navigation using smartphones. In *Proc. ACM MobiCom*, pages 512–524, 2015.

[28] L. Sun, S. Sen, D. Koutsonikolas, and K.-H. Kim. Widraw: Enabling hands-free drawing in the air on commodity wifi devices. In *Proc. ACM MobiCom*, pages 77–89, 2015.

[29] H. Wang, X. Bao, R. Roy Choudhury, and S. Nelakuditi. Visually fingerprinting humans without face recognition. In *Proc. ACM MobiSys*, pages 345–358, 2015.

[30] J. Wang, X. Chen, D. Fang, C. Q. Wu, Z. Yang, and T. Xing. Transferring compressive-sensing-based device-free localization across target diversity. *IEEE Trans. on Industrial Electronics*, 62(4):2397–2409, 2015.

[31] J. Wang, D. Fang, Z. Yang, H. Jiang, X. Chen, T. Xing, and L. Cai. E-hipa: An energy-efficient framework for high-precision multi-target-adaptive device-free localization. *IEEE Trans. on Mobile Computing*, 12(5):1–12, 2016.

[32] J. Wang, Q. Gao, P. Cheng, Y. Yu, K. Xin, and H. Wang. Lightweight robust device-free localization in wireless networks. *IEEE Trans. on Industrial Electronics*, 61(10):5681–5689, 2014.

[33] J. Wang and D. Katabi. Dude, where's my card? rfid positioning that works with multipath and non-line of sight. In *Proc. ACM SIGCOMM*, pages 51–62, 2013.

[34] J. Wang, B. Xie, D. Fang, X. Chen, C. Liu, T. Xing, and W. Nie. Accurate device-free localization with little human cost. In *Proc. ACM International Workshop on Experiences with the Design and Implementation of Smart Objects*, pages 55–60, 2015.

[35] W. Wang, A. X. Liu, M. Shahzad, K. Ling, and S. Lu. Understanding and modeling of wifi signal based human activity recognition. In *Proc. ACM MobiCom*, pages 65–76, 2015.

[36] Y. Wang, J. Liu, Y. Chen, M. Gruteser, J. Yang, and H. Liu. E-eyes: device-free location-oriented activity identification using fine-grained wifi signatures. In *Proc. ACM MobiCom*, pages 617–628, 2014.

[37] T. Wei and X. Zhang. mtrack: High-precision passive

tracking using millimeter wave radios. In *Proc. ACM MobiCom*, pages 117–129, 2015.

[38] J. Wilson and N. Patwari. See-through walls: Motion tracking using variance-based radio tomography networks. *IEEE Trans. on Mobile Computing*, 10(5):612–621, 2011.

[39] K. Wu, J. Xiao, Y. Yi, M. Gao, and L. M. Ni. Fila: Fine-grained indoor localization. In *Proc. IEEE INFOCOM*, pages 2210–2218, 2012.

[40] J. Xiao, K. Wu, Y. Yi, L. Wang, and L. M. Ni. Pilot: Passive device-free indoor localization using channel state information. In *Proc. IEEE International Conference on Distributed Computing Systems (ICDCS)*, pages 236–245, 2013.

[41] Y. Xie, Z. Li, and M. Li. Precise power delay profiling with commodity wifi. In *Proc. ACM MobiCom*, pages 53–64, 2015.

[42] J. Xiong and K. Jamieson. Towards fine-grained radio-based indoor location. In *Proc. ACM Workshop on Mobile Computing Systems & Applications*, pages 13–18, 2012.

[43] J. Xiong and K. Jamieson. Arraytrack: a fine-grained indoor location system. In *Proc. USENIX NSDI*, pages 71–84, 2013.

[44] J. Xiong, K. Jamieson, and K. Sundaresan. Synchronicity: pushing the envelope of fine-grained localization with distributed mimo. In *Proc. ACM Workshop on Hot Topics in Wireless*, pages 43–48, 2014.

[45] J. Xiong, K. Sundaresan, and K. Jamieson. Tonetrack: Leveraging frequency-agile radios for time-based indoor wireless localization. In *Proc. ACM MobiCom*, pages 537–549, 2015.

[46] L. Yang, Q. Lin, X. Li, T. Liu, and Y. Liu. See through walls with cots rfid system! In *Proc. ACM MobiCom*, pages 1–12, 2015.

[47] W. Yang, L. Gong, D. Man, J. Lv, H. Cai, X. Zhou, and Z. Yang. Enhancing the performance of indoor device-free passive localization. *International Journal of Distributed Sensor Networks*, 2015(4):1–11, 2015.

[48] M. Youssef, M. Mah, and A. Agrawala. Challenges: device-free passive localization for wireless environments. In *Proc. ACM MobiCom*, pages 222–229, 2007.

[49] D. Zhang, Y. Liu, X. Guo, and L. M. Ni. Rass: A real-time, accurate, and scalable system for tracking transceiver-free objects. *IEEE Trans. on Parallel and Distributed Systems*, 24(5):996–1008, 2013.

[50] Z. Zhou, Z. Yang, C. Wu, L. Shangguan, and Y. Liu. Towards omnidirectional passive human detection. In *Proc. IEEE INFOCOM*, pages 3057–3065, 2013.

APPENDIX

Here, we show how to calculate the DTW distance between two CSI measurements. Let $\mathbf{B}_i = \{B_i(1), \cdots, B_i(p), \cdots, B_i(K)\}$ be a set of CSI amplitudes of all K subcarriers when a target is located at location i. Consider two CSI series $\mathbf{B}_i$ and $\mathbf{B}_j$, we first construct a distance matrix $\Omega_{K\times K}$, where each element $\Omega_{p,q}$ is defined as the Euclidean distance between the two values $B_i(p)$ and $B_j(q)$:

$$\Omega_{p,q} = |B_i(p) - B_i(q)|. \tag{13}$$

The output of the DTW algorithm is a warping path $G = \{g_1, g_2, \cdots, g_L\}$ where $g_l = (p_l, q_l)$ and L is no less than K. The *DTW distance* is the minimum total cost:

$$\min_G \sum\nolimits_{l=1}^{L} \Omega_{m_l} = \sum\nolimits_{l=1}^{L} \Omega_{p_l,q_l}, \tag{14}$$

under the following constraints:

(a) Boundary constraint: $g_l = (0,0)$, $g_L = (K,K)$,

(b) Monotonicity constraint: $p_{l+1} \geqslant p_l$, $q_{l+1} \geqslant q_l$, $p_{l+1} + q_{l+1} \geqslant p_l + q_l$.